CRYSTAL GROWTH MELT FLOW CONTROL BY MEANS OF MAGNETIC FIELDS [1]

V. Galindo, G. Gerbeth
Forschungszentrum Rossendorf e.V.
P.O.Box 510119, D-01314 Dresden, Germany

W. von Ammon, E. Tomzig, J. Virbulis
Wacker Siltronic AG
P.O.Box 1140, 84479 Burghausen, Germany

Abstract

Contactless melt flow control is important in many crystal growth technologies. Typically, steady magnetic fields are used to damp convective flow. On the other hand active flow driving forces like in a rotating magnetic field can be of stabilizing character, too. We present numerical results for the combined action of steady and alternating magnetic fields for the silicon Czochralski crystal growth process. The melt flow is determined by various flow driving sources: besides the thermal convection and rotation of crystal and crucible, there are also the influence of driving and/or damping electromagnetic forces and the thermocapillarity-driven flow at the free deformable melt surface.

Keywords: crystal growth, magnetic fields, flow control

1 Introduction

The Czochralski (Cz) crystal growth technique is the main method used for producing single crystals of silicon. For a basic description of this technology we refer to [1]. Today, crystal diameters of 200 mm are an industrial standard, but a clear tendency to larger diameters like 300 mm exists. Flow and temperature fluctuations affect the homogeneity of oxygen and dopant concentration. The control of the process stability becomes more and more difficult with increasing sizes and, therefore, the wish for an external melt control is obvious. Steady (DC) magnetic fields are well-known for their overall damping action on melt motions. Because of this they have been investigated in the crystal growth context already for many years, for an overview we refer to [2]. However, for a significant flow damping and, particularly, for increasing crucible sizes the application of a DC field of sufficient strength requires large coil systems with a substantial consumption of electric power. It is therefore interesting to reconsider the well-known fact that alternating magnetic fields may drive a motion in the melt as it is long in use in inductive electromagnetic pumps or electromagnetic stirrers. Especially rotating magnetic fields have been applied recently to crystal growth processes where even a stabilizing action on the melt has been observed [3], [4]. The reason is mainly due to the fact that an electromagnetically driven flow may suitably counteract the basic buoyancy flow in the melt. It is obvious that for some optimized melt flow control one should study several combinations of steady and alternating magnetic fields very specific for the special conditions of the given growth technology. This general approach has mainly been developed by the

[1] to appear in Energy Conversion and Management

Riga team of Gelfgat [5]. Here we present some results for the combined action of AC and DC magnetic fields on the melt flow in a 4 inch Si-Cz-growth process.

2 Formulation

The geometry used to compute the flow in the melt is shown in Fig. 1.

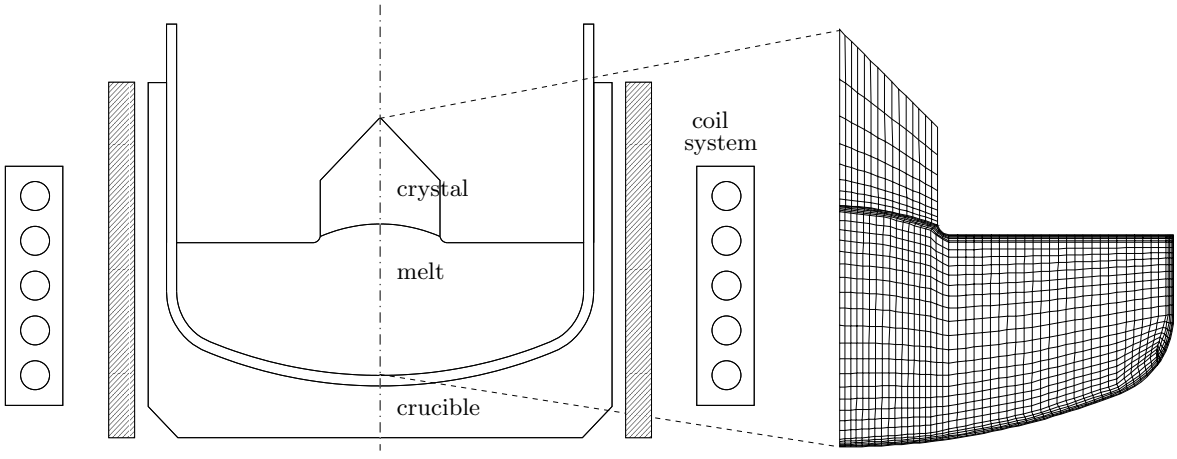

Figure 1: Sketch of the Cz crystal growth configuration (left) and computational grid (right)

The dimensions were chosen to model a Czochralski single crystal growth furnace with a crucible having a diameter of 14 inches. The crystal has a diameter of 4 inches. The problem is assumed to exhibit symmetry about the z-axis, i.e. to treat the problem as axi-symmetric and to reduce the computational mesh to the meridional $r - z$ plane.
The governing equations of the problem are as follows: With reference to Fig. 1, we consider axi-symmetric, steady flow, driven by buoyancy, thermo-capillarity, and electromagnetic forces, and heat transfer within a crucible that is heated from the sides and from the bottom. Assuming that the fluid is incompressible and that the Boussinesq approximation is valid, the time-averaged momentum, continuity, and energy equations are as follows:
Navier-Stokes (momentum) equation with electromagnetic force term:

$$\rho\,(\vec{v}\cdot\nabla)\,\vec{v} = -\nabla p + \eta\nabla^2\vec{v} - \rho\;\vec{g}\;\beta\;(T - T_0) + \vec{j}\times\vec{B} \tag{1}$$

where $\vec{v}$ is the velocity field, p the pressure, ρ the reference density, η the dynamic viscosity, β the coefficient of volume expansion, $\vec{g}$ the gravitational acceleration, $\vec{j}$ the electric current density, and $\vec{B}$ the magnetic induction (for its specification see section 4).
Mass conservation and energy transport equations:

$$\nabla\cdot\vec{v} = 0 \quad \text{and} \quad \rho\;c_p\,(\vec{v}\cdot\nabla)\,T = \nabla\cdot(k\nabla T) \tag{2}$$

where T is the temperature, c_p the specific heat, and k the thermal conductivity.
The boundary conditions are:

- no-slip condition at the crucible walls and at the interface crystal/melt with pre-given rotation rates of crucible and crystal,

- melting temperature at the interface crystal/melt,
- given heat flux distribution at the crucible walls,
- thermo-capillary conditions at the free melt surface,
- gray body radiation conditions at the melt surface and crystal sides.

The electromagnetic problem can be treated separately from the fluid flow in the low magnetic Reynolds number approximation. The magnetic Reynolds number $Rm = \mu\sigma vL$ (σ is the electrical conductivity of the melt, μ is the magnetic permeability, v and L denote characteristic velocity and length, respectively) varies in the range from 4×10^{-3} to 2×10^{-2}, which makes this approximation admissible.

3 Numerical method

The governing equations for the computation of the flow, the temperature, and the electric potential (in the case of steady magnetic fields) were solved numerically by a finite element method applying the commercial code FIDAP. Because the characteristic numbers (like the Reynolds and Grashoff numbers) are typically around the stability values (but not large enough for fully developed turbulence), we used Wilcox's low-Reynolds turbulence model (see [6]). This model belongs to the so-called two-equation group of turbulence models and is therefore closely related to $k-\epsilon$ type models. An important advantage of the Wilcox model is that it can be used to directly predict low-Re ($Re \leq 10^5$) effects on the turbulence field in the near-wall regions and does not need any (artificial) wall functions.
The two dimensional computational domain was discretized into a mesh of quadrilateral finite elements, with a finer spacing near the melt boundaries, but especially near the interface melt/crystal. It is worth noting that the Ekman layer (depth: $\delta_E = \sqrt{\nu/\Omega} \approx 0.7mm$ for $\Omega = 5\ rpm$), caused by the crystal rotation at the interface, is very thin and turns out to be crucial for the gridding of the computational domain. A very high grid refinement is necessary in that region. It is necessary to find a compromise between memory usage, computational time, and the need to find a grid-independent solution. After an analysis of the grid-dependency of the solution, we decided to use a grid with 15000 elements for all further calculations. Within this grid resolution, a completely converged steady flow and heat transfer simulation needs approximately 10 h cpu time on a SGI Origin 2000 workstation.

4 Magnetic fields

4.1 Steady magnetic field

In the case of a steady magnetic field, the induction law reduces to $\nabla \times \vec{E} = 0$. This means that an electric potential

$$\vec{E} = -\nabla\Phi$$

can be introduced.
Taking into account Ohm's law:

$$\vec{j} = \sigma\left(-\nabla\Phi + \vec{v} \times \vec{B}\right)$$

and Kirchhoff's law $\nabla \cdot \vec{j} = 0$, we obtain the following equation for the electric potential:

$$\Delta\Phi = div\left(\vec{v} \times \vec{B}\right) = \vec{B} \cdot (\nabla \times \vec{v}) - \vec{v} \cdot \left(\nabla \times \vec{B}\right) \tag{3}$$

This relation shows that in vorticity regions potential differences exist, creating a local electric field that can balance the electromotive field and allow the electric current lines to close. The relation (3) couples the electric potential, the magnetic induction, and the vorticity distribution. This equation is solved numerically in parallel to the solution of equation (1). Based on the conditions that no electric current flows through the insulating walls of the crucible and that the normal component of the current density j_n should be continuous at any interphase, the following boundary conditions for the electric potential result:

$$\frac{\partial\Phi}{\partial n} = (\vec{v} \times \vec{B}) \cdot \vec{n} \quad \text{at the crucible wall and}$$

$$(\sigma \frac{\partial\Phi}{\partial n} - \sigma_c \frac{\partial\Phi_c}{\partial n}) = \sigma (\vec{v} \times \vec{B}) \cdot \vec{n} \quad \text{at the interphase}$$

where σ_c and Φ_c denote the electrical conductivity of the crystal and the electric potential in the crystal, respectively.

In this paper, results for numerical studies are presented concerning two types of steady magnetic fields: a *homogeneous axial* and a *cusp* field. In order to generate a *homogeneous axial magnetic field* in the direction of the symmetry axis, we assumed the presence of two direct-current coils, connected in such a way that the electric current flows in the same direction in both coils. A so-called *cusp magnetic field* can be generated by means of two coil systems carrying electric currents in opposite directions. The coil configuration in the case of the *cusp field* is chosen in such a way, that the vertical component of the magnetic field is equal to zero at the melt free surface. The distribution of the field inside the melt is very inhomogeneous. This leads to a better damping effect on the meridional flow because there is no preferred field direction.

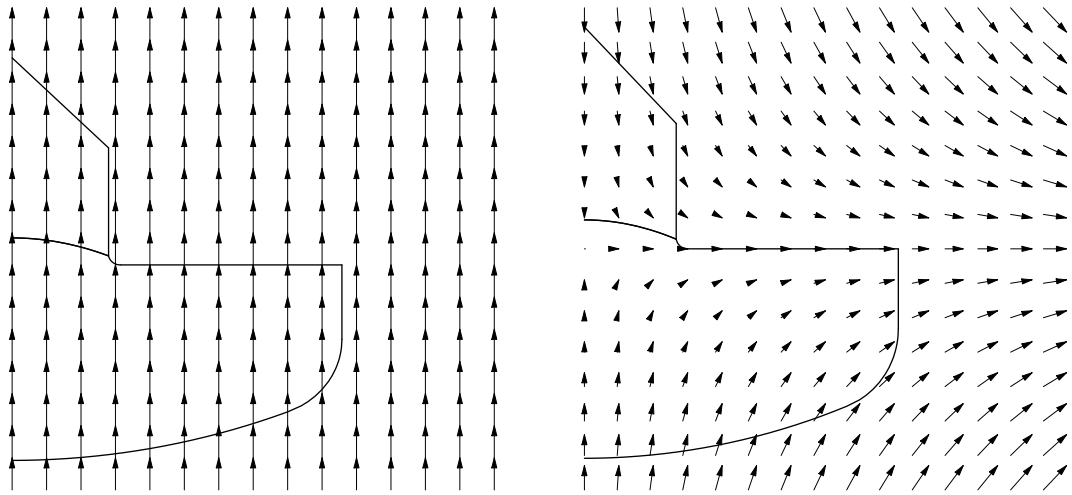

Figure 2: Steady magnetic field vector plots, Homogeneous (left) and "cusp" (right) magnetic field corresponding to the expressions 4 and 5

For simplicity we model both fields with solenoidal analytical expressions, i.e. the *homogeneous axial field* as

$$\vec{B} = B\ \vec{e_z} \tag{4}$$

and the *cusp field* as a linear field:

$$\vec{B} = B/R\ \{r\ \vec{e_r} + 2(H - z)\vec{e_z}\}, \tag{5}$$

where R and H are the radius and the height of the melt in the crucible, respectively. The corresponding vector plots are shown in Fig. 2.

4.2 Alternating magnetic field

An alternating magnetic field can be induced using a set of windings fed by an external power supply with an alternating current (AC). The electric current in different groups of windings can have a different phase. In this way, many kinds of unsteady magnetic fields (pulsating, rotating, etc.) and therefore many kinds of corresponding driving forces can be obtained. This time-dependent magnetic field induces an electric current in the conducting melt. Because of the skin effect, the magnetic field lines penetrate into the conducting material up to a skin depth of the order $\delta = 1/\sqrt{\mu\ \sigma\ \omega}$ only, where μ is the magnetic permeability, and ω the frequency of the pulsating field.

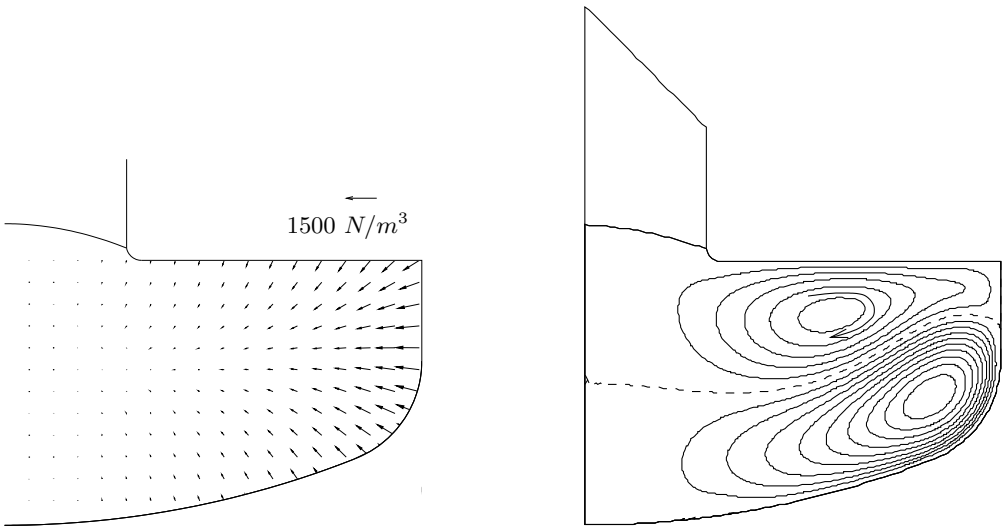

Figure 3: Lorentz force density $\vec{f_L}$ vector plot (left) and typical flow structure (right) caused by a pulsating magnetic field (it shows the double-vortex structure).

The Lorentz force $\vec{f_L} = \vec{j} \times \vec{B}$, averaged over one period, has a time-independent component since both $\vec{j}$ and $\vec{B}$ vary harmonically in time with the same frequency. This time averaged force is not irrotational. Figure 3 shows a typical distribution of the electromagnetic forces for a 50 Hz pulsating magnetic field, and the resulting typical radial-meridional flow structure .

5 Results

The parameter space of the considered problem is very large:

- rotation rates of crystal and crucible,
- heat flux in the overall facility determining the temperature boundary conditions for the buoyancy driven flow in the melt and the thermocapillary driven flow at the melt free surface,
- two types of DC magnetic fields,
- different types of AC magnetic fields with varying amplitude and frequency.

The shape of both: the crystal-melt phase boundary and the meniscus at the triple point crystal-melt-free surface have been fixed in the form of polynomial of second order since it does almost not change for varying process parameters. The obvious goal of the simulations is to identify those parameters sets providing a stable growth process with improved crystal properties like a controlled oxygen content with a good homogeneity of its axial and radial distribution. Some typical effects of the magnetic field action are shown in Fig. 4.
The main action of the AC-field consists in a flow driving mechanism superimposed on the buoyancy convection in the meridional plane. This can lead to a reversed flow direction at the free melt surface if the AC-field amplitude is sufficiently large. Without magnetic fields the meridional flow is mainly determined by buoyancy, with a strong vortex resulting in a melt flow direction from the crucible to the crystal at the free surface of the melt (not shown in Fig. 4). The AC-field primarily creates a jet at mid-height of the crucible as can be seen from the Lorentz force distribution in Fig. 3. This Lorentz force creates a double vortex structure in the melt, causing the melt at the free surface to flow from the crystal to the crucible wall, i.e., against the basic buoyant flow. Depending on the strength of the AC field this may drastically change the heat and mass transport in the meridional plane. The DC-fields have, in general, a stabilizing influence on the melt flow. This results in a general weakening of the convective motion, and (not shown in Fig. 4) in a reduction of the turbulent velocity and temperature fluctuations. A better overall damping effect is found for the cusp magnetic field since it provides no preferred direction to the flow field. In the case of a vertical homogeneous magnetic field additional instabilities may arise due to the fact that vorticity parallel to the preferred magnetic field direction is not influenced by this type of DC-fields.
These results show that different magnetic fields offer a large variety of control possibilities for the contactless optimization of heat and mass transfer processes in the silicon melt during the Cz crystal growth process of silicon.

Acknowledgements: This work has been supported by Federal Department of Education, Science, Research and Technology of FRG under contract number 01M2973A. The authors alone are responsible for the content of this publication.

References

[1] Hurle, D.T.J., Cockayne, B., *Czochralski growth*, Handbook of Crystal Growth, Vol.2, 99–211, North-Holland, Amsterdam, 1994

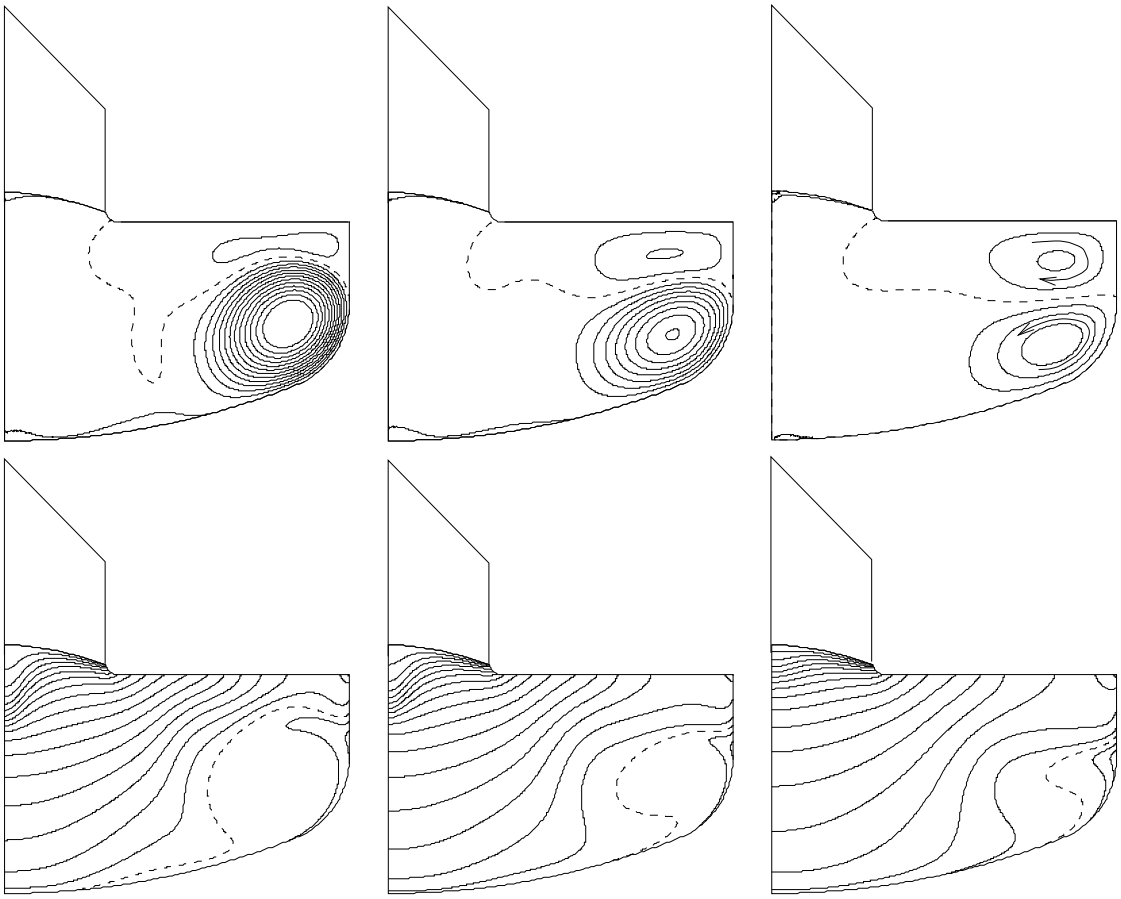

Figure 4: Flow streamlines (above) and isotherm distribution (below) by the combined action of alternating ($B_{ac} = 12\ mT$) and cusp (B_c) magnetic fields.

[2] Hurle, D.T.J., Series, R.W., *Use of a magnetic field in melt growth*, Handbook of Crystal Growth, Vol.2, 259–285, North-Holland, Amsterdam, 1994

[3] Dold, P., Benz, K.W., *Convective temperature fluctuations in liquid gallium in dependence on static and rotating magnetic fields*, Crystal Research Technology, Vol.30 (1995), 1135-1145

[4] Mößner, R., Gerbeth, G., *Buoyant melt flows under the influence of steady and rotating magnetic fields*, J. Crystal Growth, Vol.197 (1999), 341-354

[5] Gelfgat, Yu.M., Gorbunov, L.A., *Non-stationary hydrodynamics and heat/mass transfer in crystal growth MHD technologies*, Proceedings of PAMIR conference, Aussois, France, Sept.1994, Vol.1, 1–14

[6] *D. C. Wilcox*: Turbulence Modeling for CFD, DCW Industries, Inc.